JOURNAL OF MATERIALS SCIENCE 29 (1994) 15–25

Coarsening of δ′ (Al_3Li) and composite precipitates in an Al–2.5% Li–0.15% Zr alloy

M. K. AYDINOL, A. S. BOR
Metallurgical Engineering Department, Middle East Technical University, Ankara, Turkey

The early stage coarsening behaviour of δ′ (Al_3Li) precipitates and composite precipitates, consisting of β′ (Al_3Zr) core enveloped by a δ′ shell, in an Al–2.5% Li–0.15% Zr alloy has been studied at 443, 473 and 503 K by conventional transmission electron microscopy using superlattice dark-field images. Coarsening kinetics of δ′ precipitates was found to exhibit considerable deviation from the $t^{1/3}$ law corresponding to diffusion control at 473 and 503 K. This deviation may be explained either by the operation of a surface-reaction controlled coarsening mechanism represented by $t^{1/2}$ law, or by the presence of a slower precoarsening stage preceding diffusion-controlled coarsening. The particle-size distributions of δ′ precipitates were not in accordance with either the earlier theoretical predictions or the normal distribution. They were symmetrical or slightly skewed to the left, and particle sizes twice the average were observed. The coarsening kinetics of composite precipitates, was found to be rather different from that of δ′; a diffusion model which yields $t^{1/n}$ law with n changing from 1/4 to 1/6 as the coarsening progresses, was predicted. The composite precipitates have exhibited quite a narrow and rather symmetrical size distribution.

1. Introduction

Al–Li based alloys with a high technological potential in the aircraft industry due to the combination of low density and high elastic modulus also offer a scientific challenge with regard to the complex path of phase transformations involved and unexpected symmetrical particle-size distributions (PSDs) exhibited during coarsening. It is believed that, upon quenching, Al–Li solid solution almost instantaneously orders non-stoichiometrically from which non-stoichiometric δ′ (Al_3Li) Ll_2 ordered phase decomposes spinodally [1–3]. Such formed spherical δ′ precipitates exhibit an isotropic and uniform distribution due to small coherency strains, about 0.8%. The composite precipitates formed by epitaxial nucleation of δ′ phase on the already existing Ll_2 ordered β′ (Al_3Zr) particles to form a uniform shell around them, is an interesting feature of zirconium-containing Al–Li alloys. The origin of the doughnut shape of the composite precipitates in superlattice dark-field transmission electron microscope images is still a matter of debate.

The coarsening kinetics of δ′ in Al–Li based alloys has been found [4–10] to obey the classical relation

$$\bar{R}^3 = \bar{R}_0^3 + kt \quad (1)$$

where $\bar{R}$ is the average particle size at time t, $\bar{R}_0$ is the initial average particle size, and k is the rate constant that includes temperature, solute volume diffusion coefficient, surface tension and equilibrium solubility of the precipitates. The coarsening rate constant, k, for Al–Li based alloys was found [8] to depend on the lithium content of the alloy as well as on the temperature through the relation

$$\ln(kT) = -12946.16/T + 0.52(\text{wt\% Li}) - 19.97 \quad (2)$$

The activation energy for coarsening of δ′ in Al–Li alloys was found to be of the order of that for volume diffusion of lithium in solution, i.e. about 120 kJ mol^{-1} [4, 9]. The initial particle size determined from $\bar{R}^3$ versus t plots was observed to scatter around zero, ± 10 nm, with negative values as frequent as positive values [4].

The coarsening rate law given by Equation 1 is common to all contemporary theories of volume diffusion-controlled coarsening, independent of the model, diffusion geometry and mathematical approach [11–18]. The coarsening theories primarily differ in the resulting particle-size distribution (PSD), and in the magnitude of the rate constant, k. The mainframe of the modern theory of diffusion-controlled coarsening was developed independently by Lifshitz and Slyozov [11] and Wagner [12] in 1961, assuming negligible volume fraction of second-phase particles. Their analysis, known as the LSW theory, yielded an asymmetrical PSD with a tail on the left, i.e. negatively skewed, and cut-off radius at 1.5 $\bar{R}$. These predictions were not in full agreement with the experiments. Since then, attempts have been made to modify the LSW theory with more realistic geometries so that a better fit could be maintained between the experimental and theoretical PSDs. Ardell [13] has introduced the modified LSW (MLSW) theory which takes the volume fraction of the second-phase particles into ac-

0022–2461

count by modifying the diffusion geometry. PSDs predicted by MLSW theory were found to flatten and broaden with increasing volume fraction of particles but they were still asymmetrical. Comparison with the experimental data has shown that MLSW theory overestimates the effect of volume fraction on the rate of coarsening. LSW theory was further modified by adopting various diffusion geometries to rationalize the effect of volume fraction on the coarsening rate constant [14–18]. Voorhees and Glicksman [16, 17] for example, applied the multiparticle diffusion to coarsening using potential theoretic techniques. However, all the theories yielded asymmetrical PSDs except the Lifshitz and Slyozov encounter-modified (LSEM) theory presented by Davies *et al.* [18]. They have incorporated the effect of coalescence (encounter) of the particles at higher volume fractions to yield a broad and symmetrical PSD.

The rate-controlling step in the coarsening process, although less frequently encountered, may be the atom transfer across the particle–matrix interface, i.e. surface reaction, rather than volume diffusion. In the case of surface reaction-controlled coarsening, the rate equation is shown [11, 12] to be

$$\bar{R}^2 = \bar{R}_0^2 + kt \qquad (3)$$

where the rate constant, k, now also includes a surface reaction-rate parameter. The driving force of the coarsening process is still the concentration gradient between the particles due to interfacial curvature-dependent solubility of the particles. PSDs expected from a surface reaction-controlled coarsening was found [11–13] to be identical to that predicted by MLSW theory for volume diffusion-controlled coarsening at a volume fraction of one. Shiflet *et al.* [19] have proposed a coarsening model based on a ledge mechanism which gives a rate law with the exponent changing from 2 to 3 as the coarsening progresses.

The coarsened δ′ precipitates in Al–Li alloys were observed to exhibit a particle-size distribution broader and more symmetrical than that predicted by LSW or MLSW or the other modified theories, neglecting particle coalescence. The symmetrical PSDs observed in Al–Li alloys are reminiscent of the coalescence (encounter) of particles as predicted by LSEM theory, but particle aspect ratio measurements on Al–Li alloys [6] have shown that the majority of the coarsened particles have aspect ratios greater than 0.8, negating the possibility of particle coalescence. The origin of the symmetrical shape of PSDs in Al–Li alloys is not yet fully understood. Mahalingam *et al.* [8] have shown that the PSDs broaden, i.e. standard deviation of the distribution increases, the skewness of the distribution changes from negative to positive, i.e. from a tail on the left to a tail on the right, and the coarsening rate accelerates with increasing lithium content of the alloy. The normalized PSDs in Al–Li alloys were observed to achieve a steady state, independent of coarsening time and temperature in a short time. The presence of composite precipitates in zirconium-containing Al–Li alloys has caused some confusion because of the duplex nature of the PSDs with smaller δ′ precipitates and larger composite precipitates. In addition, the larger initial average size, $\bar{R}_0$, of the composite precipitates, the coarsening rate constant, k, was also greater than that for δ′ precipitates [7, 9].

The purpose of the present study was to contribute to the understanding of the coarsening behaviour of δ′ and composite precipitates in Al–Li based alloys during the early stages of ageing where classical diffusion-controlled coarsening behaviour has, possibly, not yet dominated.

2. Experimental procedure

A commercial alloy received as 1.7 mm thick sheet with composition 2.52% Li, 1.22% Cu, 0.68% Mg and 0.15% Zr by weight, was used. The alloy solution treated in the range 743–863 K were quenched to room temperature and then aged at 443, 473 and 503 K for various periods. Thin foils for transmission electron microscopy were prepared using a twin-jet polisher with a 40% CH_3COOH, 30% H_3PO_4, 20% HNO_3 and 10% H_2O solution at 273 K and were examined in Jeol 100 CXII transmission electron microscope operated at 100 kV. The particle size measurements were carried on recorded [1 0 0] and [1 1 0] superlattice dark-field images with deviation parameter, s, set to zero by locating the [2 0 0] and [2 2 0] fundamental Kikuchi lines to the positions 3/2 [1 0 0] and 3/2 [1 1 0], respectively. The micrographs were evaluated manually using an enlarger.

3. Results and discussion

Transmission electron microscopy studies on the alloy in the quenched state showed very small, about 4 nm diameter, uniformly distributed δ′ domains with low contrast and a diffuse interface in a matrix which also exhibited some contrast [3]. In the quenched state, almost all of the β′ particles were observed to be decorated with heterogeneously nucleated δ′ precipitates, either as individually distinguishable particles or in the form of a thin shell, constituting the initial stages of composite precipitate formation. Upon ageing, in addition to the increase in the average particle size, the contrast of δ′ precipitates was intensified while that of the matrix disappeared [3]. As coarsening progressed, the composite precipitates took their classical doughnut shape with a core of almost no contrast. Typical microstructures observed by TEM during the progress of coarsening are shown in Fig. 1.

3.1. Coarsening of δ′ precipitates

In the present study, the coarsening behaviour of δ′ precipitates and composite precipitates was considered separately. The coarsening data for δ′ precipitates involving the particle sizes and statistical parameters are given in Table I. The average particle-size data were plotted in Fig. 2 as $\bar{R}^3$ versus t curves according to Equation 1, for temperatures of 443, 473 and 503 K, and the corresponding regression coefficients and coarsening parameters $\bar{R}_0$ and k obtained

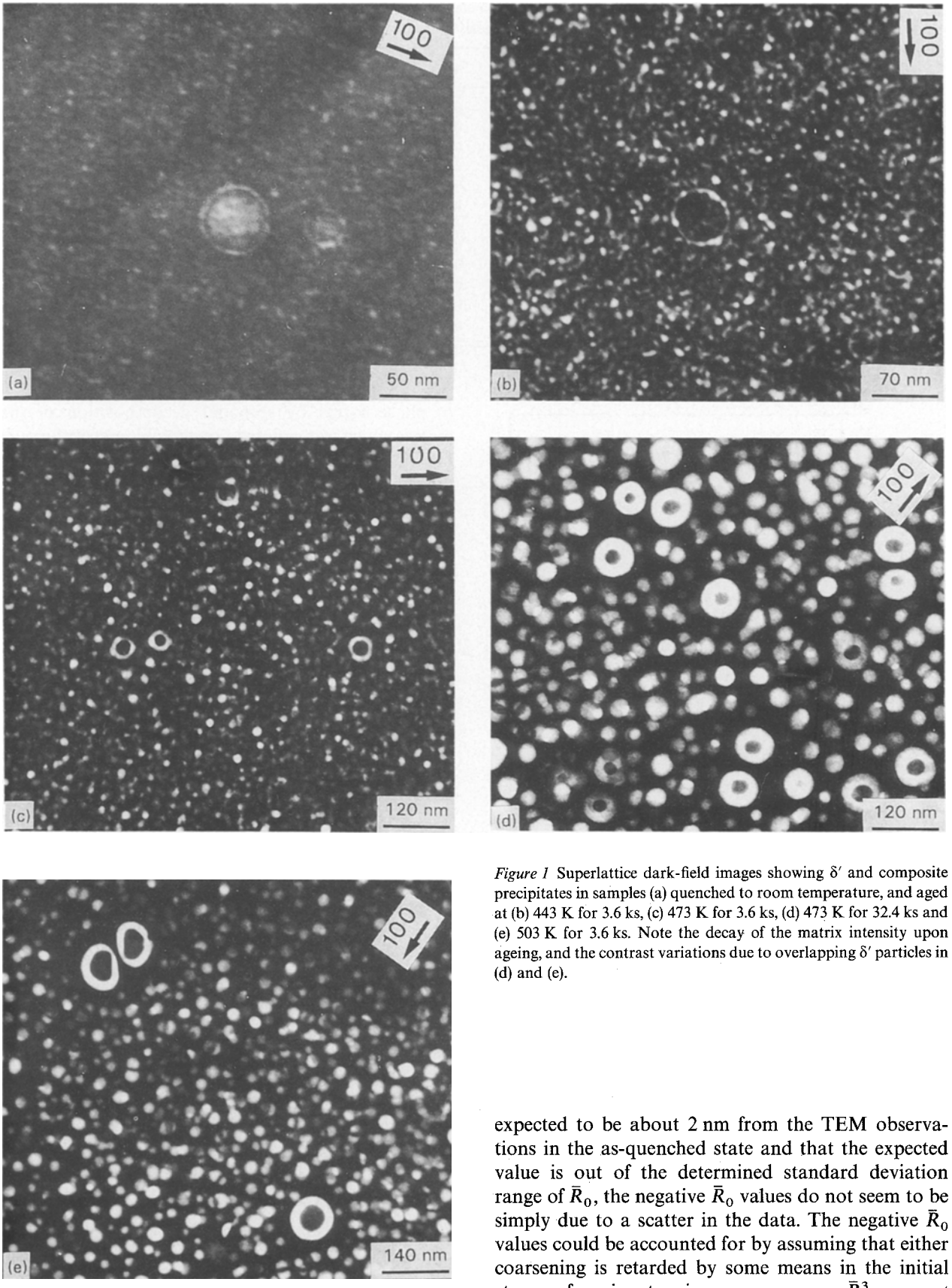

Figure 1 Superlattice dark-field images showing δ′ and composite precipitates in samples (a) quenched to room temperature, and aged at (b) 443 K for 3.6 ks, (c) 473 K for 3.6 ks, (d) 473 K for 32.4 ks and (e) 503 K for 3.6 ks. Note the decay of the matrix intensity upon ageing, and the contrast variations due to overlapping δ′ particles in (d) and (e).

by least-squares regression analysis are presented in Table II together with the standard deviations.

The outstanding feature of Fig. 2 is that the initial particle size, $\bar{R}_0$, exhibits unrealistic negative values at the ageing temperatures of 473 and 503 K. Such negative $\bar{R}_0$ values were also reported in the literature [6] and have been attributed to statistical scatter in the data. But in the present study, considering that $\bar{R}_0$ is expected to be about 2 nm from the TEM observations in the as-quenched state and that the expected value is out of the determined standard deviation range of $\bar{R}_0$, the negative $\bar{R}_0$ values do not seem to be simply due to a scatter in the data. The negative $\bar{R}_0$ values could be accounted for by assuming that either coarsening is retarded by some means in the initial stages of ageing to give a concave-up $\bar{R}^3$ versus t curve, as shown by the dotted line in Fig. 2, or a $t^{1/3}$ law is not appropriate to represent the coarsening behaviour of the alloy.

The former explanation, i.e. retardation of coarsening, would not be caused by excess quenched-in vacancy concentration or by the dissolution of small precipitates during heating to the ageing temperature, because they are, on the contrary, expected to produce an accelerating effect. It is known that in Al–Li alloys,

TABLE I Coarsening data for δ′ precipitates and statistical parameters, where $\bar{R}$ is the average particle size, s the standard deviation, $s/\bar{R}$ the coefficient of variation, skw is the skewness and krt is the kurtosis of the distribution

T(K)	t(ks)	Photos	Ppts	$\bar{R}$(nm)	s(nm)	$s/\bar{R}$	skw	krt	Class	χ^2	$\chi^2_{0.99}$
443	3.6	10	1446	3.09	0.98	0.32	0.325	−0.459	8	87.5	15.1
443	10.8	10	1670	4.31	1.22	0.28	0.322	−0.077	9	34.2	16.8
443	21.6	10	1517	5.36	1.34	0.25	−0.026	−0.207	13	103.1	23.2
443	32.4	12	1196	6.00	1.58	0.26	0.124	−0.002	11	27.1	20.1
473	3.6	12	1299	5.32	1.49	0.28	−0.117	−0.295	10	17.9	18.5
473	10.8	13	1228	8.29	2.11	0.25	−0.178	−0.241	9	17.2	16.8
473	21.6	11	1027	10.81	2.41	0.22	−0.134	−0.321	13	32.4	23.2
473	32.4	11	1170	12.84	3.00	0.23	−0.269	−0.407	13	64.0	23.2
503	3.6	12	1440	9.61	2.59	0.27	0.206	−0.351	13	53.8	23.2
503	10.8	11	1016	12.76	3.10	0.24	−0.162	−0.279	11	15.6	20.1
503	21.6	12	1019	16.87	4.60	0.27	0.050	−0.432	14	16.4	24.7
503	32.4	10	847	20.52	5.26	0.26	−0.263	−0.268	11	39.1	20.1

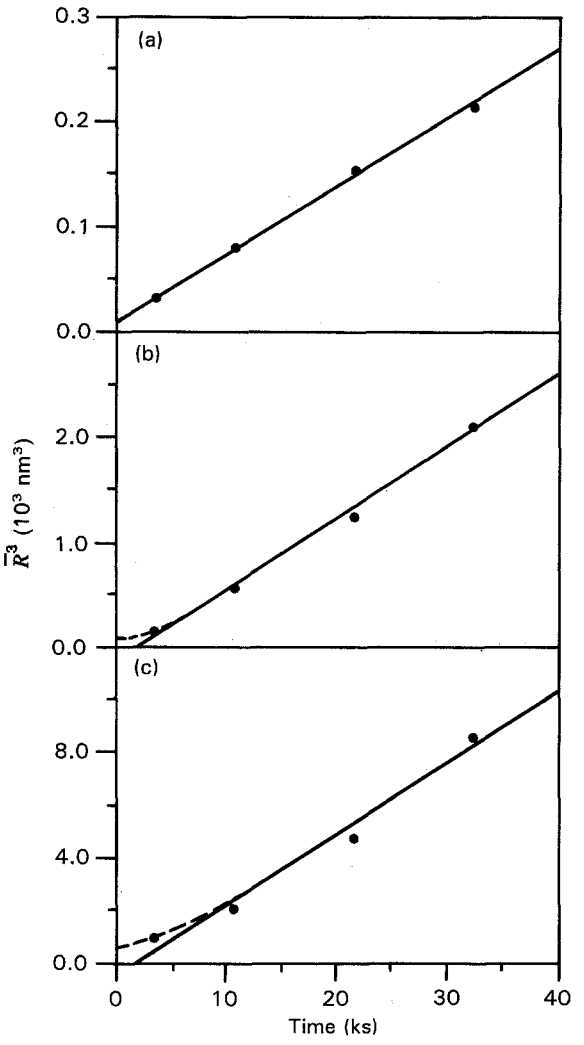

Figure 2 Coarsening data for δ′ precipitates represented as $\bar{R}^3$ versus t for coarsening temperatures (a) 443 K, (b) 473 K and (c) 503 K.

TABLE II Coarsening parameters of δ′ assuming that the relation $\bar{R}^3 = \bar{R}_0^3 + kt$ (Equation 1) is obeyed. RC = regression coefficient

T(K)	$\bar{R}_0$(nm)	k(10^{-3} nm^{3}s^{-1})	RC
443	2.05 + 1.62	6.51 + 0.21	0.999
473	− 5.19 + 4.02	68.11 + 3.20	0.998
503	− 8.05 + 8.23	270.29 + 27.54	0.990

δ′ phase forms by spinodal decomposition of the matrix which was ordered non-stoichiometrically during quenching. The spinodal decomposition starts during quenching, and in the quenched state, δ′ phase is still in the form of ordered domains with a diffuse boundary and non-equilibrium composition. The growth of the δ′ domains to transform into δ′ precipitates is expected to precede the coarsening. During this stage, lithium atoms joining with the δ′ domains by diffusion from the matrix would enrich their composition towards the stoichiometric value rather than increasing their size. This may offer an explanation of the precoarsening stage leading to the initial retardation of coarsening.

The other possibility, representation of the coarsening phenomena by the relation $\bar{R}^2 = \bar{R}_0^2 + kt$ (Equation 3) corresponding to surface reaction-controlled coarsening, is checked in Fig. 3 by plotting the square of the average particle size against the coarsening time. The regression coefficients and coarsening parameters given in Table III clearly show that the data give a better fit to the $t^{1/2}$ law, Equation 3, yielding reasonable $\bar{R}_0$ values also at temperatures of 473 and 503 K. The increase of $\bar{R}_0$ with coarsening temperature in Fig. 3 may be attributed to the dissolution of the smaller precipitates with solubilities less than the average composition of the alloy at the coarsening temperature.

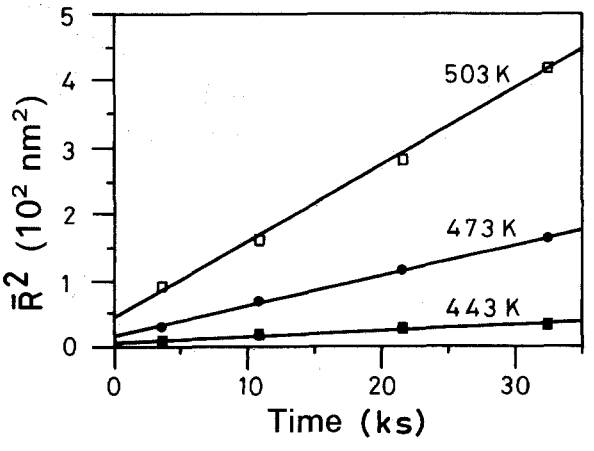

Figure 3 Coarsening data for δ′ precipitates represented as $\bar{R}^2$ versus t for coarsening temperatures 443, 473 and 503 K.

TABLE III Coarsening parameters of δ′ assuming that the relation $\bar{R}^2 = \bar{R}_0^2 + kt$ (Equation 3), is obeyed. RC = regression coefficient

T(K)	$\bar{R}_0$(nm)	$k(10^{-3}$ nm^3 s^{-1})	RC
443	2.76 + 1.28	0.91 + 0.08	0.992
473	3.81 + 1.83	4.69 + 0.17	0.999
503	6.67 + 2.87	11.44 + 0.41	0.999

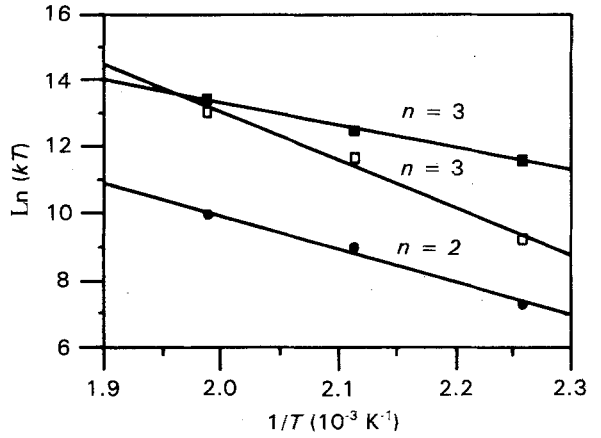

Figure 4 Temperature dependence of the (●, □) δ′ and (■) composite precipitate coarsening rate.

The rate constants, k, determined assuming diffusion-controlled coarsening represented by a $t^{1/3}$ law (Equation 1) are about three times greater than that predicted by the previous studies [6–8, 10] for alloys of similar lithium content. Compare the k values in Table II with those evaluated as 2.5×10^{-3}, 21.7×10^{-3} and 85.1×10^{-3} nm^3 s^{-1} for temperatures 441, 473 and 498 K, respectively, by Gu *et al.* [6]. The activation energy estimated, despite the limited data, from the $\ln(kT)$ versus $1/T$ plot, Fig. 4, was found to be 119 kJ mol^{-1}, which is of the order of the activation energy for substitutional lithium diffusion in aluminium and consistent with the previous studies [4, 9]. The rate constants, k, determined assuming surface reaction-controlled coarsening represented by a $t^{1/2}$ law (Equation 3) and the activation energy estimated as 82 kJ mol^{-1} from Fig. 4, are not amenable to any comparison or direct interpretation at present. The k and Q values determined do not clarify the doubt on the mechanism of initial stages of coarsening.

At this point it is not clear whether the diffusion-controlled coarsening is preceded by a slower precoarsening stage or the coarsening process is surface reaction-controlled, but the latter seems more probable with regard to the statistics of the data at 473 and 503 K. A close inspection shows that data at 403 K give a better fit to a $t^{1/3}$ law and the corresponding $\bar{R}_0$ exhibits a reasonable value, which contradicts both the precoarsening stage and the surface reaction-controlled coarsening hypothesis introduced above. The behaviour at 443 K may be explained by a change in coarsening mechanism with temperature. Recalling that surface reaction and diffusion operates in series, i.e. dependent processes, the slower one would control the overall coarsening process. Coarsening may be controlled by diffusion at 443 K and by surface reaction at the higher temperatures if the activation energy for surface reaction is higher than that for diffusion. If this is the case, the activation energies presented above are not expected to have much significance because they were obtained from data involving different mechanisms.

The present observations on coarsening of δ′ implying the possibility of a surface-controlled coarsening mechanism at shorter ageing times, are not in contradiction with the previous coarsening studies primarily confined to longer ageing times. The ledges observed on small δ′ domains by high-resolution electron microscopy [2] may be an indication of surface-controlled coarsening. On the other hand, considerable time required for the completion of the δ′ spinodal decomposition, as understood from the low contrast of δ′ particles and considerable matrix contrast in superlattice dark-field images of samples at their initial stages of coarsening [3], seems to be supporting the idea of the existence of a precoarsening stage prior to the diffusion-controlled coarsening.

The normalized particle-size distributions of coarsened δ′ precipitates are given in Fig. 5, for all coarsening times and temperatures studied. The number of particles used in constructing each PSD is listed in Table I. In plotting the PSDs, each particle size data was divided into 8–14 size classes to maintain a size distribution as smooth as possible in appearance. In fact, the size classes determined by inspection on the basis of smoothness were found also to be those that minimize the χ^2 values calculated in χ^2 tests for goodness of fit to normal distribution, as will be mentioned below. The frequency of particles was normalized by dividing the number of particles in each class by the total number of particles so that

$$\int_0^\infty g(\rho, t)\mathrm{d}\rho = 1 \qquad (4)$$

i.e. total number of precipitates involved in each PSD is normalized to unity. The particle sizes of each data set were also normalized by dividing the particle sizes by the corresponding average particle size to yield the normalized radius, $\rho = R_i/\bar{R}$. Theoretical distributions predicted by LSW and MLSW theories were superimposed as Curves a, b and c on the normalized particle size histograms in Fig. 5 for comparison purposes.

Inspection of the given experimental PSDs shows that (i) the right-hand tail extends to about $\rho = 2$, which is greater than the normalized cut-off radius predicted by the LSW and MLSW theories, (ii) the coefficient of variation, $s/\bar{R}$, which may be taken as a measure of broadness of the PSDs, is determined to be about 0.25, which is of the order of 0.215 predicted by LSW and 0.304 predicted by MLSW for second phase volume fraction, f, equal to 0.06; (iii) despite the large variation, − 0.27–0.33, in the moment coefficient of skewness, Table I, the experimental PSDs, on average,

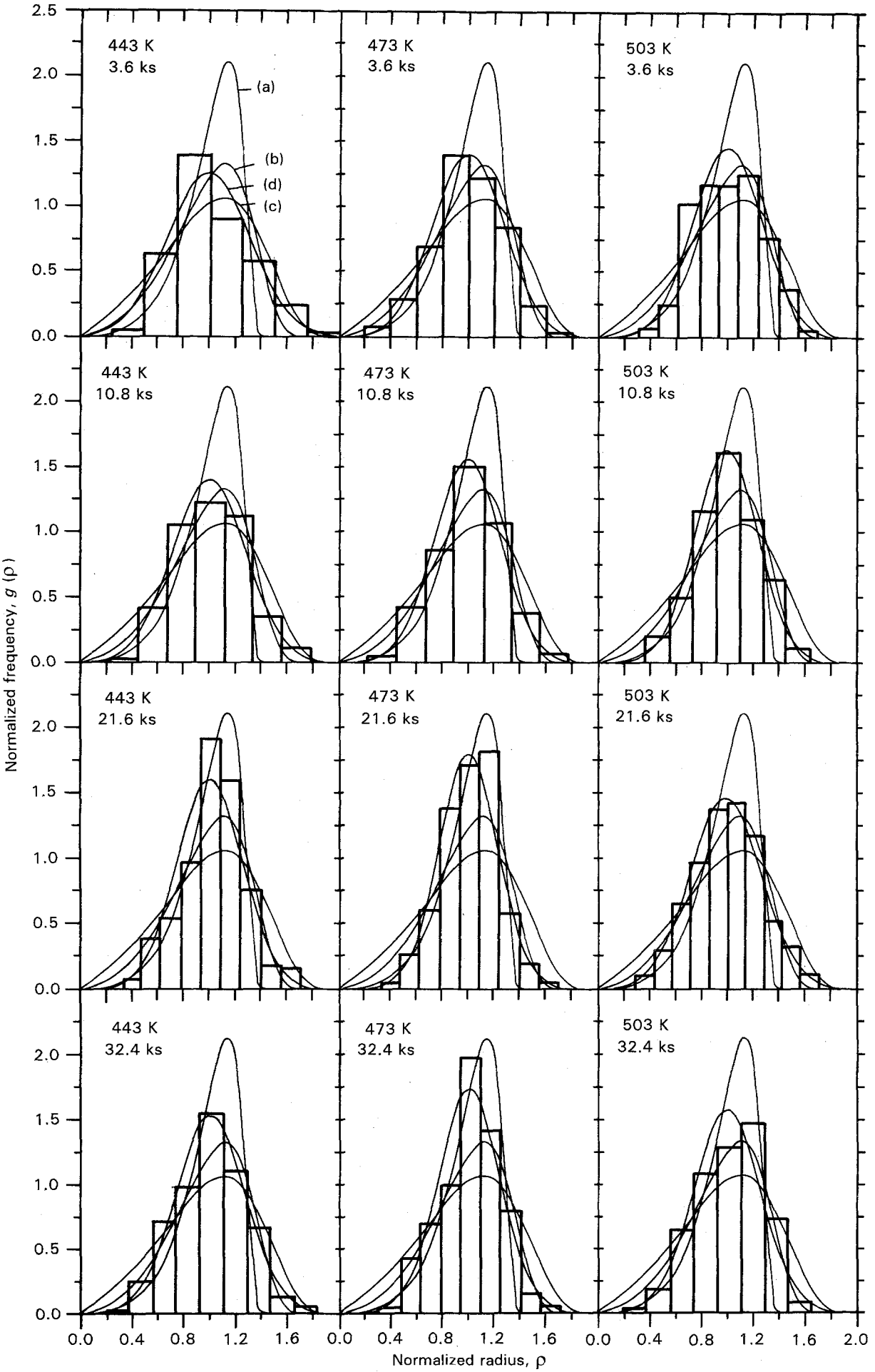

Figure 5 Normalized particle-size distribution histograms of δ′ precipitates coarsened at 403, 473 and 503 K for periods of 3.6, 10.8, 21.6 and 32.4 ks. The superimposed curves correspond to theoretical PSDs predicted by (a) LSW or MLSW ($f = 0$), (b) MLSW ($f = 0.05$), (c) MLSW ($f = 1.0$), and (d) normal distribution. Curve (c) also represents the PSD for surface reaction-controlled coarsening.

are much more symmetrical than predicted by either theory, i.e. -0.92 by LSW and -0.38 by MLSW for $f = 0.06$.

The coefficient of variation determined to be about 0.25 in the present study is in close agreement with previous studies [6, 8, 20]. The moment coefficient of skewness, on the other hand, exhibits considerable scatter in parallel with those presented in the literature; compare Gu *et al.* [7], predicting negative values, and Mahalingam *et al.* [8], predicting positive values. If the asymmetry of the PSDs are evaluated simply by comparing the position of the peak (mode) with respect to the mean, it is seen that the PSDs constructed in the present study are either symmetrical or slightly skewed to the left.

Although the symmetrical nature of the PSDs recall the LSEM theory which predicts almost symmetrical PSDs, it has not been considered in the present discussion because microstructural observations, although not quantized as done by Gu *et al.* [6], has shown that precipitate coalesence that could account for the observed distribution is negligible, Fig. 1. The eight shaped images resembling coalesced particles are, in fact, spherical δ′ precipitates at different depths overlapping in projected image. The darker and lighter contrast at the intersections depend on whether or not the overlapping variants of ordered δ′ precipitates are in phase.

Owing to the symmetrical appearance of the experimental PSDs, the particle size data were also tested for goodness of fit to normal distribution by χ^2 test [21], results of which are given in Table I together with the critical values at a level of significance of 0.01 for the corresponding size classes. χ^2 values less than the critical indicate a good fit to normal distribution at 99% confidence level. The calculated χ^2 values are mostly greater than the corresponding critical values, implying that the experimental PSDs, in general, could not be represented by a normal distribution at a 0.99 confidence level. This seems to be partly related to the scatter in the particle-size data. The negative coefficient of Kurtosis values presented in Table I also indicates that the experimental PSDs are flatter than expected from a normal distribution. For comparison, normal distribution curves were also superimposed on the particle-size histograms in Fig. 5.

Because the normalized PSDs for different coarsening times and temperatures were observed to be similar, despite the random scatter, the PSDs for all times at each temperature and also for all times and temperatures studied were combined in Figs 6 and 7, respectively, to see the overall particle-size distribution behaviour. The normalized PSDs rather than the original particle-size data were combined so that the individual PSDs contribute to the combined PSD with equal weight. The combined normalized PSDs,

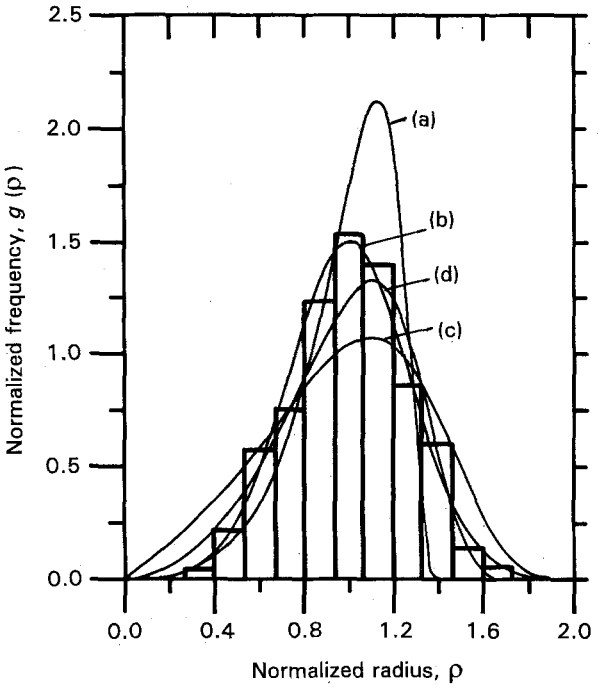

Figure 7 Combined normalized particle size distribution histograms of δ′ precipitates for all times and temperatures studied.

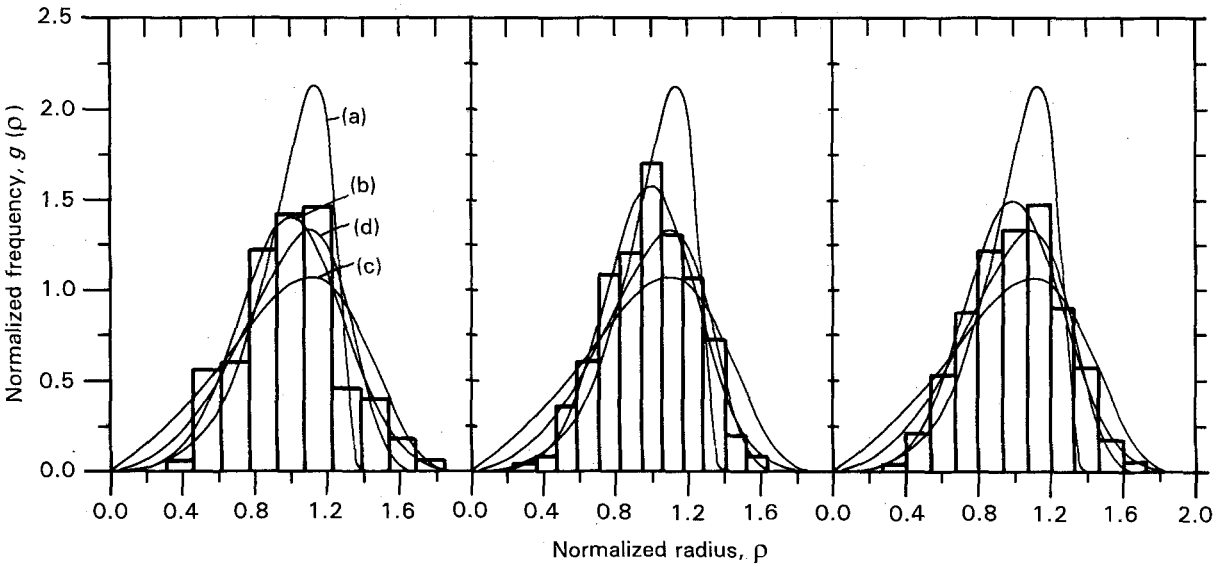

Figure 6 Combined normalized particle-size distribution histograms of δ′ precipitates for all times studied at temperatures (a) 403 K, (b) 473 K and (c) 503 K. For the superimposed curves, see caption of Fig. 5.

similar to the individual ones, exhibited considerable deviation from the LSW and MLSW models and also from the normal distribution. χ^2 test for goodness of fit to normal distribution yielded χ^2 values 391, 92, 66 and 251 for the combined PSDs for all times at 443, 473 and 503 K, and for all times and temperatures, respectively, which are considerably higher than the critical values. The significantly larger χ^2 values yielded by the combined PSDs in contrast to their smoother and more symmetrical appearance is due to the sensitivity of the χ^2 test to the number of particles involved; the larger the number of particles, the better should be the fit to satisfy the χ^2 test. The observed behaviour of PSDs is not at all clear at present.

3.2. Coarsening of composite precipitates

A survey was also conducted on the coarsening behaviour of composite precipitates formed by heterogeneous nucleation of δ′ phase on the already existing β′(Al_3Zr) particles during quenching of the early stages of ageing. In this study, coarsening of the composite precipitates was considered separate from that of the δ′ precipitates because of the much larger initial size of the composite precipitates giving rise to a duplex size distribution when considered together with the δ′ precipitates. A difficulty in studying the coarsening behaviour of composite precipitates was the inhomogeneity of the spatial and size distribution of the β′ particles constituting the core of these precipitates, which adversely affected the coarsening statistics. The inhomogeneity was particularly evident at large scale, of the order of micrometres; two- or three-fold differences were observed in the average core sizes determined using micrographs taken from different locations of the same sample. The observed inhomogeneity was also reflected in the high values of the coefficient of variation of the core size, which varies non-systematically in the range 0.25–0.48 with an average of 0.36, Table IV. Moreover, because the reason for lack of contrast at the core in TEM images is not clearly understood at present, the correlation between the actual size of the β′ core and the size of the dark central region of the composite precipitates, measured as core size, on transmission electron micrographs is not definite and probably introduces some uncertainty with regard to the core-size data.

The coarsening data on composite precipitates are given in Table IV, inspection of which shows that while the core, with an overall average radius of 13.29 nm, seems not to be affected by the coarsening process, the total composite precipitate size increases, as expected, with increasing coarsening time and temperature. The time dependence of the average composite precipitate size at coarsening temperatures of 443, 473 and 503 K are given in Fig. 8 as conventional $\bar{R}^3$ versus t curves. Despite the considerable scatter in the data due to the aforementioned local inhomogeneities, statistically a $t^{1/3}$ law was found to hold better than a $t^{1/2}$ law and, assuming that a $t^{1/3}$ law is obeyed, the coarsening rate constants were determined, approximately, as 240, 550 and 1380 nm ks^{-1} for the coarsening temperatures 443, 473 and 503 K, respectively. The rate constants are significantly larger than that for the coarsening of δ′ precipitates. Another point of interest in Table IV is the quite narrow composite precipitate-size distribution, with an average coefficient of variation equal to 0.21, in contrast to

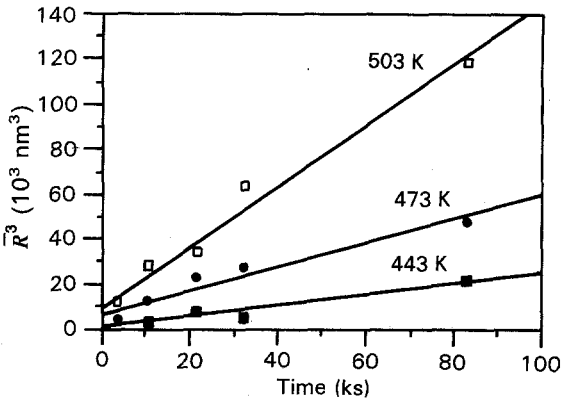

Figure 8 Coarsening data for composite precipitates represented as $\bar{R}^3$ versus t for coarsening temperatures 443, 473 and 503 K.

TABLE IV Coarsening data for composite precipitates giving the average radius, $\bar{R}$, standard deviation, s, and coefficient of variation, $s/\bar{R}$, of the β′ core size and total size

T(K)	t(ks)	Photos	Ppts	Core			Total		
				$\bar{R}$(nm)	s(nm)	$s/\bar{R}$	$\bar{R}$(nm)	s(nm)	$s/\bar{R}$
443	10.8	5	45	12.26	4.00	0.33	15.52	5.01	0.32
443	21.6	7	40	13.14	4.54	0.35	19.87	4.77	0.24
443	32.4	8	90	11.39	3.31	0.29	17.90	3.63	0.20
443	82.8	11	78	18.22	6.41	0.35	28.01	6.33	0.23
473	3.6	10	81	9.57	2.86	0.30	16.62	3.00	0.18
473	10.8	11	78	13.12	5.32	0.41	23.47	5.54	0.24
473	21.6	10	87	14.37	4.77	0.33	28.50	4.70	0.16
473	32.4	11	94	13.66	6.51	0.48	30.18	6.25	0.21
473	82.8	9	70	14.56	6.44	0.44	36.49	6.73	0.18
503	3.6	12	126	11.41	3.85	0.34	23.31	3.88	0.17
503	10.8	9	88	13.19	6.24	0.47	30.54	5.80	0.19
503	21.6	10	123	10.93	2.74	0.25	32.51	4.97	0.15
503	32.4	10	77	13.28	4.85	0.37	40.00	7.48	0.19
503	82.8	3	16	17.01	5.44	0.32	49.27	10.95	0.22

that of the core. The activation energy determined as 58 kJ mol^{-1} from the slope of the $\ln(kT)$ versus $1/T$ curve (Fig. 4), with a regression coefficient of 0.996, does not seem to have any special significance. In fact, such a good linear fit to the $\ln(kT)$ versus $1/T$ relation with such limited data and hence the calculated activation energy, seem to be spurious.

Neither the $t^{1/3}$ time dependence nor the $\{\exp(-Q/RT)\}/T$ type temperature dependence employed above following the previous studies on the subject [7, 9] has firm theoretical basis because the coarsening geometry of the composite precipitates in the range studied is different from the physical model of classical coarsening that yields the above given time and temperature dependences. Coarsening of the composite precipitations, although also driven by the concentration gradient due to interfacial curvature-dependent solubility, as in classical diffusion-controlled coarsening, is more similar to diffusional precipitate growth with regard to the diffusion field geometry. Until the later stages of coarsening, where most of the δ′ precipitates are either consumed by the larger composite precipitates or coarsened to sizes comparable to that of the composite precipitates, the composite precipitates are separated by matrix regions with finely dispersed δ′ precipitates so that the diffusion fields of the composite precipitates do not interact. Because the composite precipitates are the largest ones in the neighbourhood, all of them coarsen steadily by consuming the nearby δ′ precipitates leading to a precipitate-free zone (PFZ) formation in the area around them. The PFZ width for a given composite precipitate size may be calculated by a simple mass balance involving the volume fraction of δ′ precipitates. Such a calculation has shown that the PFZ width/composite precipitate size ratio increases rapidly during the initial stages of formation but then approaches a constant value which is a function of the δ′ precipitate volume fraction, Fig. 9.

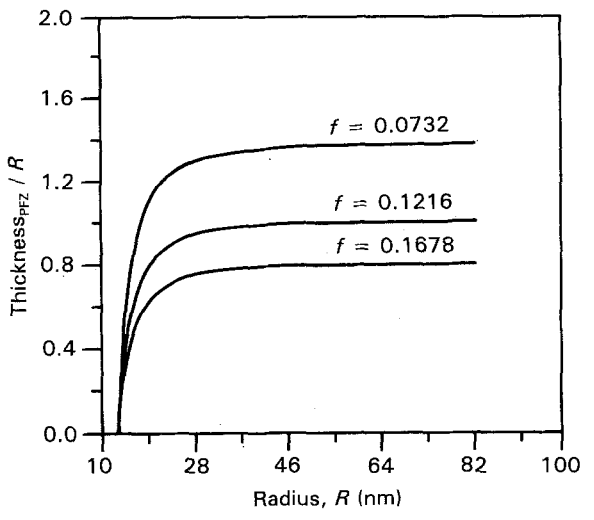

Figure 9 Development of the precipitate-free zone around the composite precipitates during coarsening as a function of composite precipitate size for various volume fractions of δ′ precipitates, i.e. 0.168, 0.122 and 0.073 corresponding to those at temperatures (■) 443, (●) 473 and (□) 503 K, (shown in Fig. 8) respectively.

The coarsening rate of composite precipitates is expected to be quite high due to the presence of an ample number of δ′ precipitates around each composite precipitate as a source of lithium atoms and also due to the large size difference between the composite and δ′ precipitates. However, by the progression of coarsening, in addition to the coarsening of δ′ precipitates to reduce the size-dependent concentration difference, the quickly developed PFZ increases the diffusion distance, causing the coarsening rate to decrease rapidly with time.

The coarsening of composite precipitates could be modelled either (i) in terms of particle to particle interactions between the composite and neighbouring δ′ precipitates if the δ′ precipitates are widely separated, or (ii) as the δ′ precipitates at the outer rim of the PFZ forming a constant composition front from which lithium atoms diffuse towards the composite precipitate through the PFZ if the δ′ precipitates are finely dispersed with a small interparticle distance, Fig. 10.

The rate equation for the coarsening of composite precipitates could be derived by solving the multibody diffusion problem for the former model, or by solving the diffusion problem involving two moving interfaces with position (time)-dependent concentrations, in spherical coordinates, for the latter model. But such analytical solutions were found to be a formidable task and have not been attempted. Instead, a simplified numerical approach was employed; the steady-state solution for diffusion from individual neighbouring δ′ precipitates towards the composite precipitate, for the former model

$$Q = (4\pi R_2^2)\left(\frac{3f}{2\pi R_{\delta'}^2}\right)(2\pi R_{\delta'}^2)D(C_2 - C_1)\mathrm{d}t \quad (5)$$

or diffusion across a spherical wall (corresponding to the PFZ in the present case)

$$Q = 4\pi\left(\frac{R_1 R_2}{R_2 - R_1}\right)D(C_2 - C_1)\mathrm{d}t \quad (6)$$

was iterated for small times, 100 s, using a personal computer. In Equations 5 and 6, Q is the number of atoms transferred in time period $\mathrm{d}t$, D is the lithium diffusion coefficient, $R_{\delta'}$, R_1 and R_2 are the average radii of the δ′ precipitates, composite precipitate and the PFZ, respectively, and C_1 and C_2 are the corresponding size-dependent solubilities. The change in the composite precipitate size and the PFZ width due to lithium atom transfer across the PFZ was calculated in each iteration using Equation 5 or 6 and mass balance, respectively, and the new values were used as the input of the next iteration. The size-dependent solubilities of the precipitates, C_1 and C_2, employed in Equations 5 and 6 were also recalculated in each iteration using the Gibbs–Thompson relation

$$X(R) = X(\infty)\exp\left[\frac{1 - X(\infty)}{0.25 - X(\infty)}\frac{2\gamma V_m}{kTR_{\delta'}}\right] \quad (7)$$

where $X(R)$ and $X(\infty)$ are fractional solubilities of δ′ precipitates of radius $R_{\delta'}$ and infinity, respectively, V_m is the atomic volume of lithium atoms, γ is the surface tension and k is the Boltzmann constant.

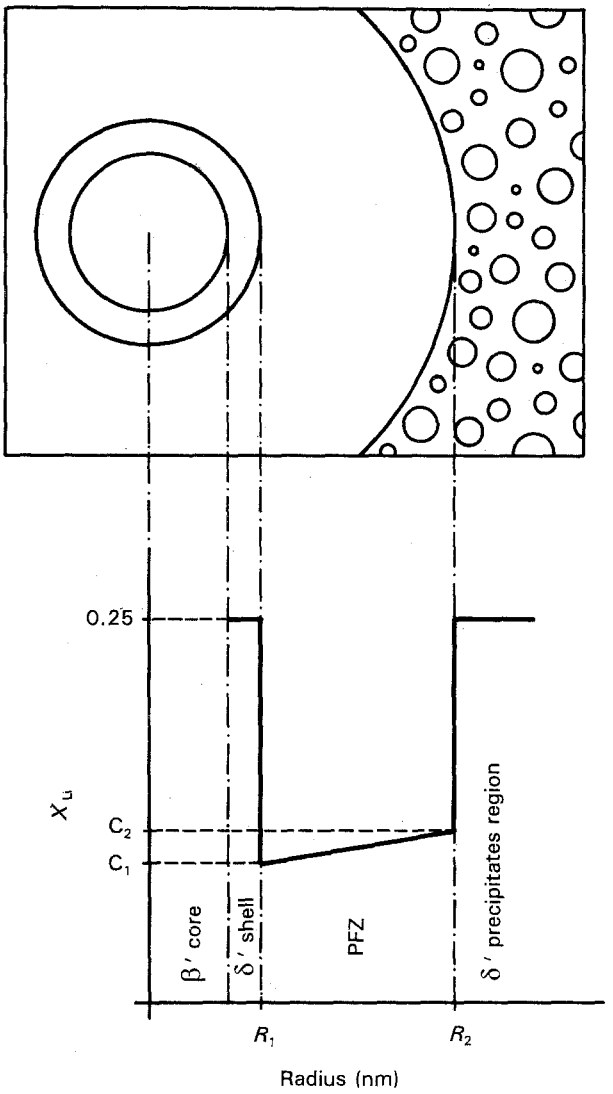

Figure 10 The lithium concentration profile modelling the diffusion-field geometry of coarsening composite precipitates separated by finely dispersed δ′ precipitates beyond the precipitate-free zone.

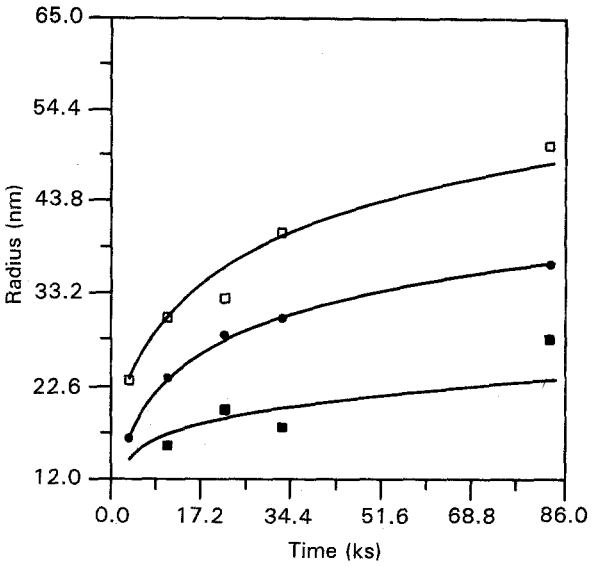

Figure 11 The output of the diffusion model predicted for the coarsening of composite precipitates assuming the geometry given in Fig. 10 (curves) compared to the experimental results (points) at coarsening temperatures (■) 443, (●) 473 and (□) 503 K. The surface tension values were taken as 0.17 J m^{-2} for 443 and 473 K and as 0.08 J m^{-2} for 503 K in model calculations.

The values of the parameters used in the simulation process are taken as β′ core size = 13.3 nm, $D = 4.5 \times 10^{14} \exp(-33\,300/1.98\,T)$ nm^2 s^{-1}, $V_m = 0.0165$ nm^3, and $X(\infty) = 0.056$ at 403 K, 0.068 at 473 K and 0.080 at 503 K, where D is taken from Costas [22]. Because the surface tension values presented in the literature vary by more than an order of magnitude, e.g. 0.014 J m^{-2} [23], 0.19 J m^{-2} [24] and 0.24 J m^{-2} [4], it was taken as a variable and systematically changed in the range 0.01–0.24 J m^{-2} in the simulation process to determine the value leading to the best fit between the model and the experimental data. The parameter that is most uncertain in the later model was the concentration at the outer rim of the PFZ, C_2, where the δ′ particles progressively become smaller and then dissolve. As a first-order approximation, C_2 at a given time was calculated using the Gibbs–Thompson relation with δ′ particle radius equal to the average size determined from the δ′ coarsening data of the previous section.

Both models were found to yield similar time dependence but the results differed slightly in magnitude. The output of the latter model compared to the experimental data is given in Fig. 11 as $\bar{R}$ versus t plots for temperatures 443, 473 and 503 K, using the surface tension values that give the best fit. The correlation between the model and the experimental results is rather good, probably due to the independent choice of the surface tension values, which were found to lie in the range 0.08–0.17 J m^{-2} for both models but giving slightly lower values in the given range for the coarsening temperature 503 K, which implies that either the models are slightly overestimating the coarsening rate at the higher temperatures or, less probably, the data are in some error due to lithium loss during the higher temperature experiments. Keeping in mind the limitations of the model due to their approximate nature, the δ′/matrix surface tension seems to be of the order of 0.1 J m^{-2}, which is in the range predicted by the previous studies [4, 23, 24]. The models were found to overestimate the coarsening rate also in the initial stages of coarsening, where the PFZ is just forming and the diffusion geometry is not stabilized and is more complex than assumed by the models. To prevent the deficiencies of the models at short ageing times, the computer simulations were started from 3600 s, as from Fig. 11.

Overall, within limitations, the models were found to represent satisfactorily the coarsening of composite precipitates. Computer simulations for different periods at the temperatures employed in the present study have shown that the coarsening kinetics of composite precipitates may be approximated by a power law, $\bar{R} \propto t^n$, where n changes from 1/4–1/6 with the progress of coarsening.

The insignificance of the rate constants and activation energies calculated above and presented in the literature assuming a $t^{1/3}$ law is evident from the foregoing discussion.

The particle-size distribution of the composite precipitates is also expected to be totally different from

that of the δ′ precipitates and from the theoretically predicted distributions for coarsening because of the basic differences in the diffusion geometry. Computer simulations employing the experimentally determined normal distribution of β′ core size as the initial condition, have shown that, within the time and temperature range of the present study, the shape and standard deviation of the distribution remains almost the same, independent of time and temperature of coarsening, i.e. the initial distribution simply shifts to the right with coarsening time. This obviously results in narrowing of the normalized PSD, which corresponds to a decrease in the coefficient of variation, $s/\bar{R}$, owing to the increase in mean particle size, as experimentally observed and presented in Table IV. This was not something unexpected, because all the composite precipitates steadily grow during ageing in contrast to the continuous widening of PSD of δ′ precipitates due to concurrent growth and shrinkage.

4. Conclusions

Investigation of the coarsening behaviour of δ′ precipitates and composite precipitates in an Al–2.5% Li–0.15% Zr alloy by conventional TEM techniques has led to the following conclusions.

1. Coarsening data for δ′ precipitates at temperatures of 473 and 503 K exhibited a better fit to the $t^{1/2}$ law, $\bar{R}^2 = \bar{R}_0^2 + kt$, with respect to the $t^{1/3}$ law, $\bar{R}^3 = \bar{R}_0^3 + kt$, which may be interpreted as operation of surface reaction-controlled coarsening mechanism or by presence of a precoarsening stage in diffusion-controlled coarsening.

2. Particle-size distribution of δ′ precipitates were not in accordance with the previous theoretical predictions or the normal distribution, and the cut-off radius was observed to be at about $2\bar{R}$.

3. Coalesence of δ′ precipitates during coarsening was not observed in TEM studies.

4. The coarsening rate of composite precipitates was almost an order of magnitude larger than that for δ′ precipitates. Solution of the model predicted for the coarsening of composite precipitates by an iterative method on a computer has shown that the composite precipitate size is approximately proportional to t^n, with n changing from 1/4–1/6 as the coarsening progresses.

5. Particle-size distribution of the composite precipitates was quite narrow, with a coefficient of variation of about 0.2.

References

1. A. G. KHACHATURYAN, T. F. LINDSEY and J. W. MORRIS Jr, *Metall. Trans.* **19A** (1988) 249.
2. V. RADMILOVIC, A. G. FOX and G. THOMAS, *Acta Metall.* **37** (1989) 2385.
3. M. K. AYDINOL and A. S. BOR, in "Proceedings of EMAG'91 Conference", Bristol, England, September, 1991, edited by F. J. Humphreys (IOP Publishing Ltd., Bristol, 1991) p. 253.
4. B. NOBLE and G. E. THOMPSON, *Met. Sci. J.* **5** (1971) 114.
5. D. B. WILLIAMS and J. W. EDDINGTON, *ibid.* **9** (1975) 529.
6. B. P. GU, G. L. LIEDL, J. H. KULWICKI and T. H. SANDERS Jr, *Mater Sci. Eng.* **70** (1985) 217.
7. B. P. GU, G. L. LIEDL, T. H. SANDERS Jr and K. WELPMANN, *ibid.* **76** (1985) 147.
8. K. MAHALINGAM, B. P. GU, G. L. LIEDL and T. H. SANDERS Jr, *Acta Metall.* **35** (1987) 483.
9. P. L. MAKIN and B. RALPH, *J. Mater. Sci* **19** (1984) 3835.
10. O. JENSRUD and N. RYUM, *Mater. Sci. Eng.* **64** (1984) 229.
11. I. M. LIFSHITZ and V. V. SLYOZOV, *J. Phys. Chem. Solids* **19** (1961) 35.
12. C. WAGNER, *Z. Elektrochem.* **65** (1961) 581.
13. A. J. ARDELL, *Acta Metall.* **20** (1972) 61.
14. A. D. BRAILSFORD and P. WYNBLATT, *ibid.* **27** (1979) 489.
15. K. TSUMURAYA and Y. MIYATA, *ibid.* **31** (1983) 437.
16. P. W. VOORHEES and M. E. GLICKSMAN, *ibid.* **32** (1984) 2001.
17. *Idem, ibid.* **32** (1984) 2013.
18. C. K. L. DAVIES, P. NASH and R. N. STEVENS, *ibid.* **28** (1980) 179.
19. G. J. SHIFLET, H. I. AARONSON and T. H. COURTNEY, *ibid.* **27** (1979) 377.
20. Y. TOMOKIYO, K. YAHIRO, S. MATSUMURA, K. OKI and T. EGUCHI, in "Proceedings of the International Symposium on Dynamics of Ordering Processes in Condensed Matter", Kyoto, Japan, August 1987, edited by S. Komura and H. Furukawa (Plenum Press, New York, 1987) p. 233.
21. M. R. SPIEGEL, in "Schaum's Outline Series: Statistics" (McGraw Hill, New York, 1972) p. 201.
22. L. P. COSTAS, USAEC Rep. DP-813 (1963) US Atomic Energy Commission.
23. S. F. BAUMAN and D. B. WILLIAMS, *Acta Metall.* **33** (1985) 1069.
24. M. FURUKAWA, Y. MIURA and M. NEMOTO, *Trans. Jpn. Inst. Metals* **26** (1985) 230.

Received 27 November 1991
and accepted 24 March 1993